Review Article: Gas and vapor sorption measurements using electronic beam balances

David L. Minnick, Tugba Turnaoglu, Maria Alejandra Rocha, and Mark B. Shiflett

Citation: Journal of Vacuum Science & Technology A **36**, 050801 (2018); doi: 10.1116/1.5044552

View online: https://doi.org/10.1116/1.5044552

View Table of Contents: https://avs.scitation.org/toc/jva/36/5

Published by the American Vacuum Society

Review Article: Gas and vapor sorption measurements using electronic beam balances

David L. Minnick, Tugba Turnaoglu, Maria Alejandra Rocha, and Mark B. Shiflett[a)]
Department of Chemical and Petroleum Engineering and Center for Environmentally Beneficial Catalysis, University of Kansas, Lawrence, Kansas 66045

(Received 13 June 2018; accepted 7 August 2018; published 30 August 2018)

The beam balance is one of the oldest known measuring instruments. Until the 20th century, balances had been the most sensitive and precise instruments used for scientific measurements. The original balances used a beam supported at the center with pans hung from cords on both ends. The modern electronic beam balances still resemble those original designs; however, the resolution, accuracy, and capabilities have been significantly improved. This review provides a short introduction to the history of beam balances followed by a detailed description of three gravimetric microbalances manufactured by Hiden Isochema for measuring gas and vapor sorption in a variety of materials.
https://doi.org/10.1116/1.5044552

I. INTRODUCTION

The invention of the beam balance most likely originated with the development of commerce and trade within the Neolithic era around 5000 B.C.[1] The oldest artifacts of beam balances and weights, which were first used by the Egyptians, are from about 3300 B.C. The history is so long that the word "balance" comes from the Latin word *bilanx*, which means "two pans." The earliest physical balances used a beam which was supported at the center with pans hung from both ends by cords. A later improvement in the design by the Romans, about 100 A.D., used a pin through the center of the beam for the central bearing.[1] The development of balances with regard to sensitivity, precision, and ease to operate occurred slowly over millennia until technical requirements for chemistry, toward the end of the 18th century, led to significant advancements in resolution to maximum load ($<10^{-9}$). The modern analytical balance design is credited to the Scottish chemist Joseph Black who developed the technique using a light weight, rigid beam supported on a knife-edge fulcrum.[1] Although there have been hundreds of improvements on the equal arm balance, the fundamental design served the scientific community for over 200 years from 1750 to 1950; however, the measurements were time consuming and tedious. The typical resolution in mass was about 0.1 mg and the most advanced designs could measure mass changes of about 0.001 mg (1 μg).[2] Some of the technical improvements during this period included pan brakes, magnetic damping of beam oscillation, built-in weight sets operated by dial knobs, and microprojection reading of the angle of beam inclination. The balances were often enclosed in wood and glass cases to minimize air currents and humidity effects. Ehrhard Mettler began the commercialization of the single-pan weighing balance in 1947, which remained the standard until the development of electronic balances around 1970.[3]

Between 1981 and 1988, a UK Science and Engineering Research Council (SERC) project funded the development of the first computer controlled gravimetric microbalance at the University of Birmingham. The initial design, developed by Benham and Ross, was unique as it incorporated a computerized data acquisition system, automated pressure control, the ability to obtain measurements at pressures up to 1 MPa, and a balance dampening system to increase the stability of the mass measurements.[4] The initial concept was further refined and developed into the intelligent gravimetric analyzer (IGA) instrument which became commercially available from Hiden Analytical in 1992 and is described in detail in Sec. II. Hiden Analytical (now Hiden Isochema Ltd.) further developed their instrumentation platform with the addition of the Dynamic Vapor Sorption Analyzer (IGAsorp) instrument in 1997 which is specifically designed for vapor sorption measurements and is described in Sec. III. Most recently, in 2013, Hiden introduced the magnetically coupled XEMIS microbalance which can operate at pressures up to 20 MPa and handle corrosive gases as described in Sec. IV.

II. INTELLIGENT GRAVIMETRIC ANALYZER

The IGA microbalance is a unique instrument which can measure changes in sample mass as a function of temperature, pressure, and gas composition. The analyzer can handle multiple, controllable, gas inlets and can be integrated with a mass spectrometer. The IGA method provides real-time gravimetric data to determine both kinetic parameters and predict sorption equilibrium simultaneously.[5] For this reason, the IGA instrument has been utilized to study gas sorption for a broad range of materials including solid adsorbents [e.g., zeolites, carbons, metal organic frameworks (MOFs), etc.] and ionic liquids (ILs).[6] During the time period from 1992 to 2004, approximately 100 papers were published using the IGA microbalance, and research publications have continued to increase

[a)]Author to whom correspondence should be addressed: mark.b.shiflett@ku.edu

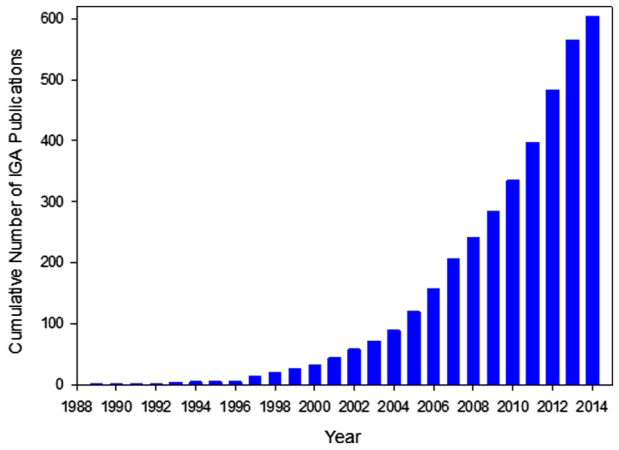

FIG. 1. Cumulative papers published using an IGA gravimetric microbalance by publication year.

exponentially as shown in Fig. 1. It is currently estimated that more than 1000 papers have been published with results measured using an IGA microbalance.

Gravimetric microbalance instruments were initially developed to measure the chemisorption of hydrogen in pure metals and metal alloys and to gravimetrically track the pressure-composition-temperature curves.[4] Many early IGA microbalance papers published between 1994 and 2013 investigated the adsorption of H_2 for storage applications on a variety of materials such as carbons,[7–21] metal organic frameworks,[22–48] molecular sieves,[49–51] silicas,[52–55] and zeolites.[56–62] Today, significant research on gas adsorption continues to be published using the IGA microbalance. For example, several researchers have recently investigated solid adsorbents for CO_2 capture applications[63–69] and others have used the IGA microbalance to measure the sorption capacity for a variety of other noncorrosive gases.[70–77]

While most IGA microbalance measurements are focused on the solubility and diffusivity of gases, the instrument can also be configured with a liquid reservoir to study the sorption properties of aqueous[49,78–86] and organic[87–93] vapors. The IGA instrument can be operated in two modes for vapor sorption analysis. First, the IGA can be operated in "static mode" where a vapor is generated using the vacuum system by creating a controlled partial pressure of the liquid. Alternatively, the system can be configured in "dynamic mode" where an inert gas (i.e., helium) contacts the liquid and generates a saturated vapor stream with a specified partial pressure controlled by the temperature of the vapor generation cell. In both configurations, the vapor is admitted to the sample environment, where it contacts the adsorbent and the mass is measured. Fletcher *et al.* demonstrated that operating the balance in static and dynamic modes does not significantly impact the thermodynamic vapor sorption capacity of the sorbent.[94] However, multiple studies have shown that a helium carrier gas decreases the kinetic rate of adsorption for vapor species by disrupting the mean free path of the sorbate molecules, thus reducing the rate of gas phase diffusion.[49,94]

While gravimetric techniques are particularly useful for obtaining single component gas sorption measurements, there is a significant need to study competitive adsorption with mixed gases. Unfortunately, few techniques exist which can measure simultaneous adsorption of mixed gases since decoupling the mass contributions of each sorbate is difficult.[95] Fletcher *et al.* devised a method of measuring the competitive adsorption of a gas + vapor mixture using the IGA microbalance in a two-step process.[94] First, adsorption of the mixed sorbate species is accomplished by flowing the mixture over the adsorbent. Subsequently, temperature programmed desorption (TPD) is used in conjunction with an on-line mass spectrometer to quantify the relative amounts of each volatile component present. The method successfully demonstrated a technique to simultaneously measure multicomponent sorption using the IGA microbalance with an on-line mass spectrometer; however, continued development in this area is needed.

In addition to gas sorption experiments, the IGA microbalance can be utilized for material characterization experiments including thermal gravimetric analysis (TGA)[96,97] and TPD.[98,99] These techniques are especially useful when the instrument is coupled to an on-line mass spectrometer. The combined methods provide simultaneous gravimetric and gas phase analysis for the complete characterization of a sample.

The IGA microbalance has also been used to measure the solubility of gases in a new class of materials called ionic liquids. ILs are salts which have melting points below 100 °C. A unique property of ILs is their extremely low vapor pressure (i.e., < 0.001 Pa), which makes it possible to measure the gas solubility using a gravimetric microbalance (i.e., negligible volatility). Maginn, Brennecke, and coworkers were the first to study the solubility of CO_2 in imidazolium based ILs using an IGA microbalance.[100–102] Research continues to be conducted in this area with recent studies focused on new ILs with enhanced CO_2 solubility.[103–106] The IGA balance has been used to study the solubility of a wide range of gases in ILs including: H_2, O_2, N_2, CO, CO_2, Ar, Xe, Kr, SO_2, H_2S, N_2O, NO_2, NH_3, H_2O, hydrocarbons, and hydrofluorocarbons.[107] The solubilities of more than 20 fluorocarbon gases in ionic liquids have also been measured using an IGA microbalance.[5,108–116] The solubility results have been used to characterize hydrogen-fluorine bond interactions between hydrofluorocarbon gases and fluorinated IL anions with applications for the selective separation of refrigerant gases.[112]

The IGA microbalance was used to measure the solubility of CO_2 in 1-hexyl-3-methylimidazolium bis(trifluoromethylsulfonyl)imide [hmim][Tf_2N] as part of an International Union of Pure and Applied Chemistry (IUPAC) study targeting "Thermodynamics of Ionic Liquids, Ionic Liquid Mixtures, and the Development of Standardized Test Systems."[117–120] The results of this study were used by IUPAC as a standard for gas solubility measurements in ILs.[118] The solubility of CO_2 was recently measured again in [hmim][Tf_2N] and compared with the original IGA IUPAC results as shown in Fig. 2. The [hmim][Tf_2N] + CO_2 solubility results agreed to within ± 0.5 mol.% with the published data highlighting the accuracy and reproducibility that can be achieved using an IGA microbalance. Therefore, the IGA can be used to verify the accuracy of other gas sorption measurement techniques.[121]

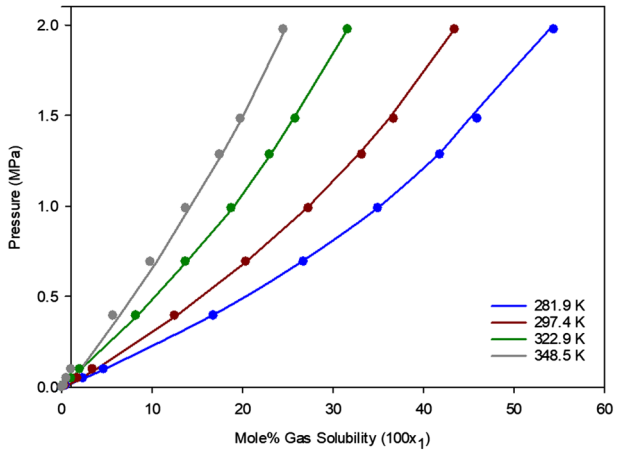

FIG. 2. Comparison of CO_2 solubility in the ionic liquid [hmim][Tf_2N]. Lines represent IUPAC data measured by Shiflett *et al.* (Ref. 118). Symbols represent present experimental data.

The IGA microbalance, shown in Fig. 3, is composed of a balance beam which is connected to a sample cup and counterweight by a series of hangdown wires and hooks. The IGA microbalance operates at pressures ranging from vacuum (10^{-10} MPa) to 2 MPa and temperatures between 77 and 1273 K. Application specific sample cup geometries exist for the IGA including Pyrex bulbs for liquid samples, stainless-steel baskets and screens for solid materials, and quartz containers for high-temperature applications ($T >$ 1000 K). The IGA instrument utilizes a force balance method to determine the mass of a sample in a pressure and temperature controlled environment by detecting incremental changes in the position of the balance beam which moves in response to buoyancy and gravity forces acting on the components within the system. The IGA balance has a mass resolution of 0.1 μg and is capable of measuring gas solubility with an accuracy better than ± 0.5 mol.% (± 0.1 mass%) for sorption experiments with ILs. The IGA can be used with a range of noncorrosive gases and vapors in combination with solid and liquid phase samples (i.e., <100 mg).

The IGA microbalance is fully automated and controlled using the HIsorp software program providing precision pressure and temperature control. The IGA system is equipped with a pair of foreline and turbomolecular pumps which can

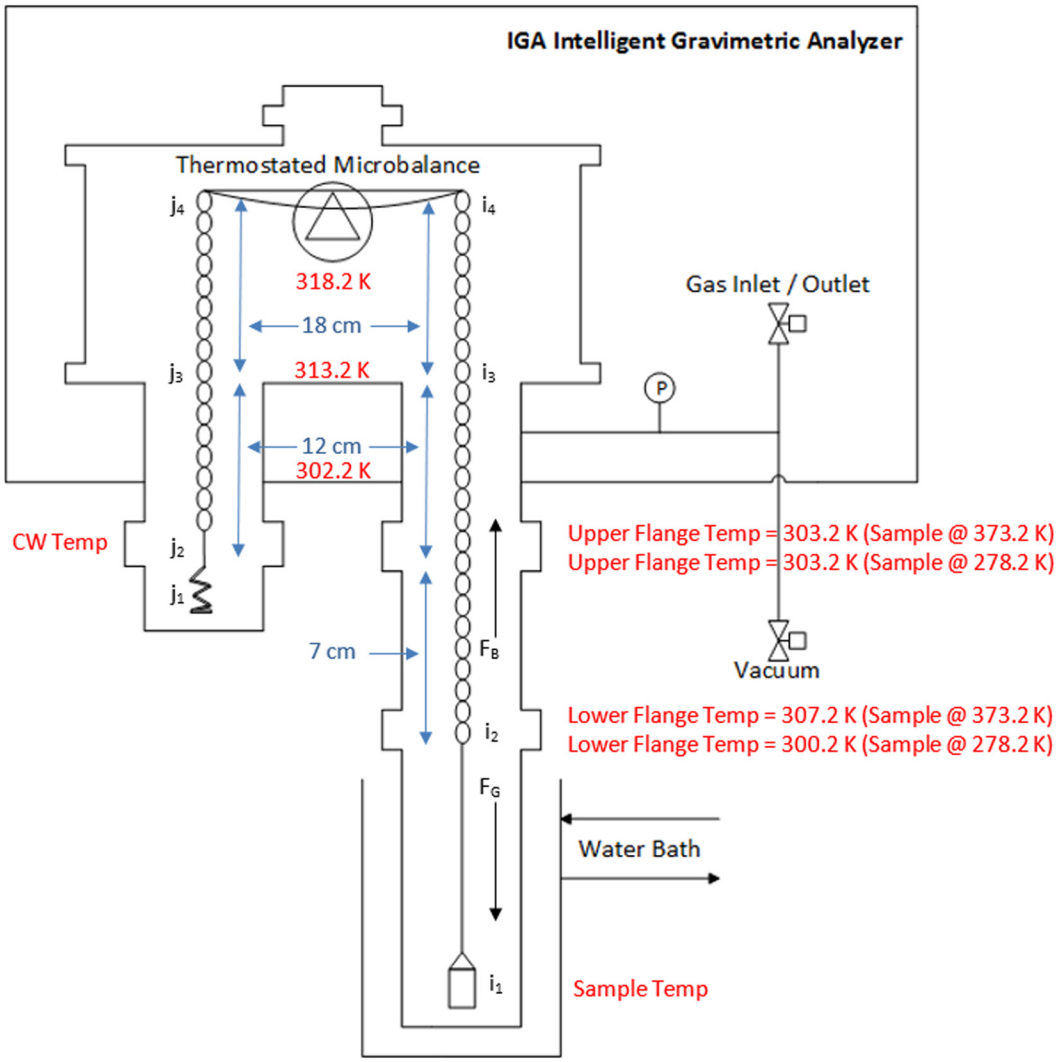

FIG. 3. Hiden IGA gravimetric microbalance schematic with temperature profile and component labels. Nomenclature is described in Table I, see text for explanation of temperature profile shown.

achieve vacuum pressures of approximately 10^{-10} MPa. The vacuum pumps are especially useful for *in situ* sample pretreatment, where volatile impurities including moisture can be removed from the sample prior to analysis. The pressure within the balance is regulated by a pair of motorized admit and exhaust valves and is measured by a pressure transducer which maintains an accuracy of ± 0.05% of range. The IGA instrument can be equipped with multiple pressure transducers for accurate low (< 0.1 MPa) and high pressure (0.1–2 MPa) measurements. Gas sorption measurements can be conducted in "static mode" where a specified gas pressure is maintained within the system by the admit/exhaust valves. Alternatively, the IGA can be operated in "dynamic mode" where a mass flow controller (MFC) regulates the flow rate of a gas (max 500 $cm^3\ min^{-1}$) which passes over the sample and is exhausted out of the balance. When operated in dynamic mode, the IGA balance can be coupled to an on-line mass spectrometer through a heated transfer line for direct gas phase analysis. In this configuration, dynamic mode is especially advantageous for TGA and TPD experiments.

Temperature control within the microbalance can be divided into three primary zones including the balance, counterweight, and sample chambers. The balance chamber is continuously maintained at a constant temperature by a band heater (i.e. 318.2 K). Both temperatures are measured by resistance temperature detector (RTD) probes and recorded in real time by the HIsorp software program. The sample temperature is measured by an *in situ* RTD (optional thermocouple) temperature probe which is accurate to ± 0.1 K. A variety of attachments are available to regulate the sample temperature including a jacketed water bath for sample temperature control between 278 and 358 K (± 0.05 K). A furnace is also available for high-temperature applications up to 773 K when used with the stainless-steel sample vessel and 1273 K when used with a specialized quartz sample vessel (± 1 K). For increased flexibility, a combined water bath and furnace heater (combi-bath) is available, which combines the water bath and furnace into a single unit permitting temperature control over a broad range from 278 to 773 K. Finally, a cryofurnace is available for subambient temperature measurements as low as 77 K (± 1 K).

Calculating gas solubility measurements using the IGA instrument requires solving a force balance to correct for the buoyancy forces acting on the microbalance components. The buoyancy correction is formulated according to Archimedes' principle, which states that the buoyant force applied to an object acts in an upward direction and is equivalent to the volume of the displaced fluid. A general equation used to compute the buoyant force (F_b) acting on an object is shown in Eq. (1), where g is the gravitational acceleration, V_i is the volume of the object, and ρ_g is the density of the gas surrounding the object at a known temperature and pressure (T,P). Gas phase density data was calculated using the NIST REFPROP v.9.1 database which contains thermodynamic and transport properties for more than 80 compounds:[122]

$$F_b = Buoyant\ Force = gV_i\rho_g = g\frac{m_i}{\rho_i}\rho_g(T, P). \tag{1}$$

Components within the microbalance are constructed from materials with known densities. The volume of the components can be computed from mass (m_i) and density (ρ_i) data as shown in Eq. (1). A summary of the components within the IGA microbalance which are used in the buoyancy correction is shown in Table I.

The general force balance equation used to correct the gas solubility for buoyancy is shown below:

$$\sum_i m_i{*}g(sample\ \ side) - \sum_j m_j{*}g(counterweight\ \ side) = balance\ \ reading{*}g. \tag{2}$$

Expanding Eq. (2) to include each microbalance component in Table I and canceling the gravity terms yields a mass balance equation which is shown below:

$$\sum_{i=1} m_i - \sum_{j=1} m_j - \sum_{i=1}\frac{m_i}{\rho_i}\rho_g(T_i, P) + \sum_{j=1}\frac{m_j}{\rho_j}\rho_g(T_i, P) + m_s + m_a - \frac{m_s}{\rho_s(T_s)}\rho_g(T_i, P) - \frac{m_a}{\rho_a(T_a)}\rho_g(T_i, P) - C_f(T_s, P) = balance\ reading. \tag{3}$$

In addition to the previously defined terms, m_s is the mass of the sample, m_a is the mass of the absorbed gas, and C_f is a balance correction factor used to account for nonideal changes in the balance reading due to pressure and temperature effects. The correction factor is measured by conducting a preliminary experiment without the sample at each experimental temperature and pressure condition using the selected gas.

The correction factor is minimally affected by the approximation of temperature within the IGA system. For instance, if the balance beam is maintained at a constant temperature of 318.2 K, while the counterweight is at the lab temperature (e.g., 298.2 K) and the sample temperature changes based on the experimental setpoint; then temperature gradients exist within the balance which impact the density of the gas interacting with the hangdown wire components. To obtain an accurate temperature profile, an infrared thermometer was used to measure the temperature at multiple points along the sample and counterweight sides of the balance. For the sample side, multiple experimental temperatures were explored to investigate the impact of sample temperature on the stainless-steel tube which contains the upper sample side gold hangdown chain. Similar studies were also conducted on the counterweight side of the balance and the temperature profile results are shown in Fig. 3. The experimentally measured temperatures and hangdown wire lengths were used to develop two empirical correlations to approximate the temperature gradients in the balance. Utilization of these

TABLE I. Standard IGA microbalance components included in buoyancy correction.

Subscript	Component	Material	Weight (g)	Density (g/cm^3)	Temperature (K)
s	Sample	Variable	m_s	ρ_s	Sample Temp
a	Gas	Variable	m_a	ρ_a	Variable
i_1	Sample container	Pyrex	1.3915	2.23	Sample Temp
i_2	Lower hangdown wire	Tungsten	0.0572	19.04	Sample Temp
i_3	Upper hangdown chain	22 Ct. gold	0.3028	11.10	T Profile i
i_4	Sample side balance hook	Tungsten	0.0059	19.04	Balance Temp
j_1	Counterweight (CW)	316 SS	1.5679	7.89	CW Temp
j_2	CW hook	Tungsten	0.0059	19.04	CW Temp
j_3	CW hangdown chain	22 Ct. gold	0.2401	11.10	T Profile j
j_4	CW balance hook	Tungsten	0.0059	19.04	Balance Temp

equations for computing the buoyancy of the upper sample and counterweight gold hangdown chains reduces the magnitude of the correction factor. With the incorporation of the temperature profile, the correction factor is typically less than 0.1 mg and its magnitude is directly proportional to pressure while inversely proportional to temperature.

The absorption of a gas into a liquid sample can result in the liquid volume expanding (i.e., volume expansion). For ionic liquids, the volume expansion can be significant, especially when investigating the solubility of hydrofluorocarbon gases. The volume expansion of 1-ethyl-3-methylimidazolium bis(trifluoromethylsulfonyl)imide [emim][Tf_2N] with chlorodifluoromethane (R-22) was measured using a volumetric view cell. The results demonstrated that the [emim][Tf_2N] sample expanded by 134% at 298.2 K and 0.890 MPa, where the solubility of R-22 was measured to be 81.8 mol.%. This data point represents an extreme case, where the experimental pressure of R-22 is close to its saturated vapor pressure at 298.2 K (P_{Sat} = 1.0439 MPa). Under these conditions, volume expansion of the IL is maximized as the gas becomes increasingly dense and its solubility approaches 100%. In general, volume expansion is primarily a function of gas solubility and is therefore greatest at low temperatures and high pressures.

For gravimetric microbalance measurements, volume expansion has an effect on the buoyancy of the liquid sample which directly impacts the calculated gas solubility. For instance, the volume expansion of [emim][Tf_2N] + R-22 at 298.2 K and 0.890 MPa results in a 0.5 mol.% difference between the uncorrected and volume expansion adjusted solubility measurements. Shiflett and Yokozeki previously showed that volume expansion of an IL could be approximated using a mole fraction average of the pure component molar volumes:[5]

$$\tilde{V}_m(T, P) = \tilde{V}_{IL}(1 - x) + \tilde{V}_g(x). \tag{4}$$

Equation (4) is used to compute the average molar volume of the mixture, where $\tilde{V}_i = MW_i/\rho_i$ and x represents the mole fraction of the gas solute in solution ($MW_i \equiv$ molecular weight of component i). The volume of the gas expanded liquid phase can be computed by Eq. (5), where V_m is the volume of the liquid mixture:

$$V_m(T, P) = \tilde{V}_m(T, P)\left[\frac{m_s}{MW_{IL}} + \frac{m_a}{MW_g}\right]. \tag{5}$$

Finally, the mass of the adsorbate (m_a) can be determined using Eq. (6) and can be substituted into Eq. (3) to compute the volume expansion corrected solubility value:

$$\frac{m_s}{\rho_s(T_s)}\rho_g(T_s, P) + \frac{m_a}{\rho_a T_a}\rho_g = V_m(T, P)\rho_g(T, P). \tag{6}$$

A series of volume expansion measurements were conducted using three ionic liquids and two compressed gases to study the ability of the model to approximate mixture molar volume (i.e., volume expansion). Figure 4 displays the mixture molar volume of the IL + compressed gas as a function of gas solubility. The experimental results demonstrate three important conclusions. First, Eq. (4) computes the experimental molar volume for an IL + gas binary system at pressures up to 2.0 MPa with a maximum deviation between

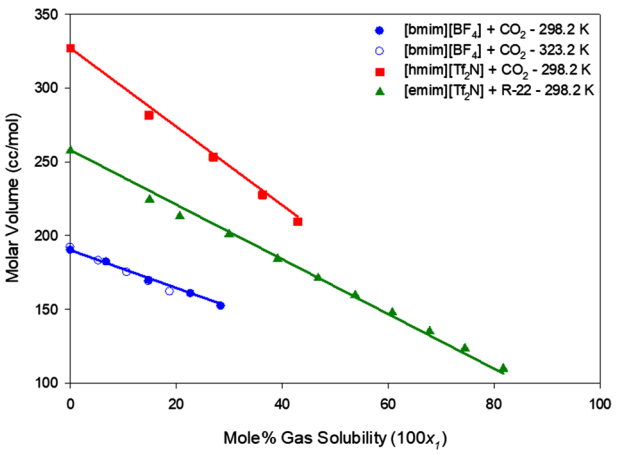

FIG. 4. Molar volume of ionic liquid–compressed gas mixtures as a function of gas solubility at pressures up to 2.0 MPa. Symbols represent experimental data points; lines represent approximate mixture molar volume calculated by Eq. (4).

the computed and experimental data points of less than ± 2%. The accuracy of the model alleviates the need to experimentally measure the volume expansion of each gas + IL system studied in the gravimetric microbalance. Second, the molar volume of the mixture is primarily dependent on gas solubility. This result is particularly important because the pure component density of the gas is only available at temperatures below the critical temperature (T_c). Therefore, at conditions where the sample temperature is greater than the critical temperature of the gas, one can adequately use mixture molar volume results from subcritical temperature measurements for the gas + IL pair. This observation was recently validated by comparing the mixture molar volume results for the 1-butyl-3-methylimidazolium tetrafluoroborate [bmim][BF_4] + CO_2 system at 298.2 and 323.2 K, where the computed mixture molar volume results at 298.2 K adequately matched the results at 323.2 K. Finally, the average molar volume calculation is valid for a range of solvent (IL) and solute (gas) pairs. For instance, the model accurately predicted the mixture molar volume of two IL systems (i.e., [bmim][BF_4] and [hmim][Tf_2N]) with CO_2 as well as the [emim][Tf_2N] system with chlorodifluoromethane (R-22) as shown in Fig. 4.

The experimental results shown in Fig. 4 were obtained at pressures up to 0.89 and 2.0 MPa with R-22 and CO_2, respectively. In this pressure range, the average molar volume calculation was accurate to within ± 2% of the experimental data. However, at high pressures ($P > 2.0$ MPa), experimental mixture molar volume data deviated from the model. For instance, the mixture molar volume of the [hmim][Tf_2N] + CO_2 system was measured at pressures up to 6.0 MPa using a volumetric view cell.[123] At the highest pressures, the model underpredicted the mixture molar volume by approximately 7%, likely due to nonideal mixing properties of the solution. Volume expansion (i.e., mixture molar volume) is a secondary adjustment for IGA microbalance measurements and is incorporated into the buoyancy correction. Therefore, small errors in the calculation of mixture molar volume do not significantly impact the calculation of gas solubility. For instance, a 10% change in the mixture molar volume changes the computed gas solubility by ± 0.1 mol.%.

III. DYNAMIC VAPOR SORPTION ANALYZER (IGAsorp)

Hiden IGAsorp combines humidity and temperature control with precise weight change measurements. The instrument was first introduced in 1997 and has been used for a variety of applications. Analysis of the equilibrium and kinetic measurements allows for material characterization of solid and liquid samples, such as measuring the solubility of water and organic vapors and calculation of mass transfer coefficients.

Fundamental, NASA funded, research conducted by Robertson and Bish investigated the stability of perchlorates when exposed to water. The IGAsorp results indicated that the perchlorate hydration state changes at select phase transitions which was used to indicate a potential source of water on Mars.[124] The IGAsorp has also been used for quality control studies in the pharmaceutical, electronics, and construction industries to understand the impact of moisture on water sensitive products. For example, pharmaceutical researchers have used the IGAsorp to study the interaction of moisture with layered materials. The results showed that water reduces the integrity of adhesion between bilayer tablets.[125] Scientists have also measured the surface of polyethylene terephthalate films treated with amines using Hiden's IGAsorp, assessing the moisture capacity and biocompatibility of the products.[126] The IGAsorp has also been used to investigate the moisture sorption capacity of electromechanical materials whose dielectric properties can be significantly impaired at high water content.[127–129] Researchers at the Forest Products Lab have used the IGAsorp to measure the water vapor permeance in their innovative paper layered insulation system.[130] In addition to observing direct moisture trends, researchers have also used the IGAsorp to calculate the mass transfer coefficients of water in polymers such as polydimethylsiloxane and polyurethanes[131–134] and in residential materials such as insulations.[130,135]

The IGAsorp is an ultrasensitive electrobalance with 0.05 μg resolution and a 1 g weighing capacity. It operates at temperatures ranging from 278 to 573 K (with the optional preheater) and ambient pressure. Similar to the IGA microbalance (Sec. II), the IGAsorp has a sample side (i) and a counterweight side (j), as shown in Fig. 5. On each end of the balance beam, a tungsten hook connects to a gold chain. At the opposite end of each gold chain, a second tungsten hook connects the counterweight and the sample cup. The counterweight is made of stainless-steel wire, and different types of sample cups are available depending on the application. For solid samples, a cone-shaped mesh container is used, which allows vapor to contact increased sample surface area. Additionally, a Pyrex glass bulb is used to study liquid samples. Both containers are shown in Fig. 5.

Relative humidity (% RH) is controlled within the IGAsorp by measuring a combination of dry and wet nitrogen (N_2) streams. Dry N_2 enters the instrument and is divided into two streams. The flow rate of each stream is controlled using an MFC. One of the N_2 streams passes through a solvent reservoir, where it is saturated with the solvent at a set temperature. The dry N_2 then combines with the wet N_2, and the mixed stream flows into the sample chamber. A relative humidity sensor with a measurement accuracy of ± 1% RH from 0% to 90% RH and ± 2% RH from 90% to 95% RH and a platinum RTD temperature probe (± 0.1 K) located inside the sample chamber provide proportional integral differential feedback control to the MFCs.

The IGAsorp uses different modes to operate over a broad range of relative humidities. The conventional method is the "climate mode" which uses a flow rate of 250 ml/min N_2 and is optimal for measuring relative humidities ranging from 2% to 95%. Alternatively, the "climate XT" mode is used for measurements at low humidity conditions (0–5% RH) and uses a flow rate of 500 ml/min N_2. In climate mode, the

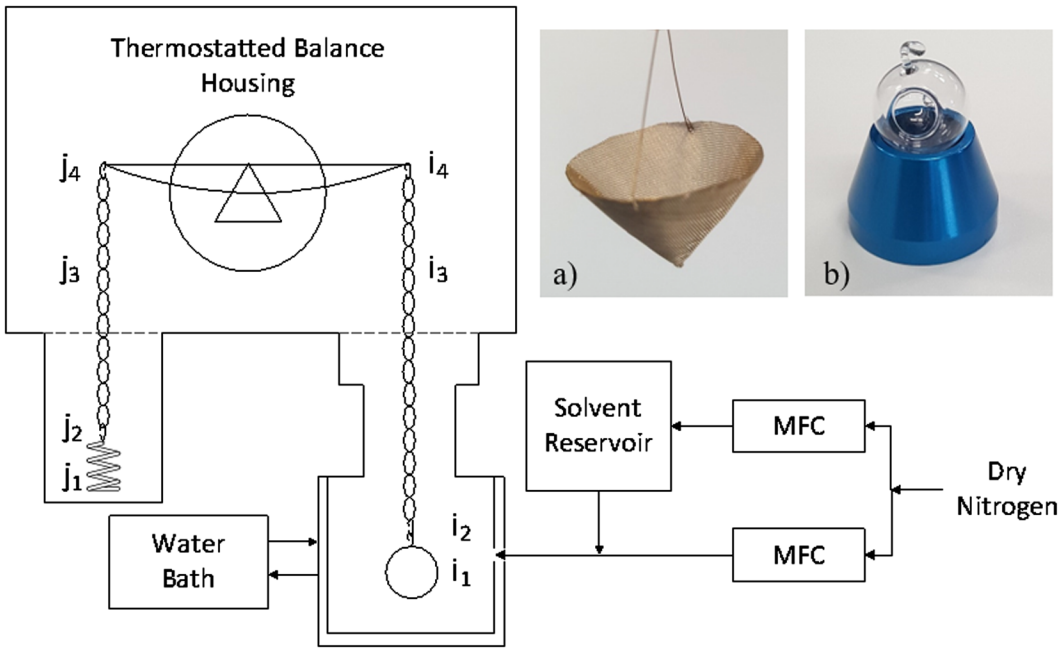

FIG. 5. Hiden IGAsorp gravimetric microbalance schematic with component labels. Nomenclature is described in Table II. Inset (a) stainless-steel mesh container used for solid samples and (b) Pyrex bulb in a sample holder used for liquid samples.

sample chamber is controlled by a water bath for temperatures between 278 and 358 K (± 0.05 K) and by a heater (which is included with the IGAsorp-XT or as an accessory to the IGAsorp) for measurements at temperature up to 623 K (±1 K). The solvent reservoir temperature is regulated only by the water bath. In climate mode, the sample chamber and the solvent reservoir are controlled at the same temperature using the water bath. Consequently, in controlling the humidity, the percent of wet flow rate (wet flow/total flow × 100%) will be similar to the % RH. Climate XT mode uses a different approach, as it controls the temperature of the solvent reservoir using the water bath but controls the sample chamber temperature using the heater. This method allows the IGAsorp to reach low humidity values while maintaining a sufficient vapor flow rate. Importantly, the HIsorp software program intelligently controls the IGAsorp reservoir temperature to achieve the target flow rate and relative humidity conditions.

In addition to data acquisition and control, the HIsorp software predicts sorption equilibrium in real time. The default method uses the Linear Driving Force exponential model, shown below:

$$y = y_0 + \Delta y\left(1 - e^{-k_L(t-t_0)}\right), \tag{7}$$

where y is the total weight of the sample including the sorbed species, y_0 is the initial weight, Δy is the weight change, t is the time, t_0 is the initial time, and k_L is the mass transfer coefficient. The predictive model reduces experiment time, as the thermodynamic IGAsorp measurements are done at atmospheric pressure and can take days to weeks to reach equilibrium.

Microgravimetric balances are extremely sensitive instruments and measurement error can easily be introduced through buoyancy changes and electrobalance disturbances. Not correcting for these errors can lead to large inaccuracies in mass measurements (0.1–5 mg).[136] The IGAsorp design minimizes experimental error. For instance, temperature and pressure fluctuation effects on the electrobalance can essentially be ignored as the balance housing is kept at 343 K (± 0.1 K) and is constantly purged with dry nitrogen to prevent humidity changes near the balance beam. Additionally, drag effects can be assumed negligible as the sample cup is tarred under flowing nitrogen gas. This environment is identical to what is used when obtaining sample measurements suggesting that the only observable mass difference must be due to the sorption of the solute. Finally, the buoyancy is corrected using a force balance and the volume expansion is accounted for assuming additive molar volumes, as discussed in Sec. II. Two opposing forces act on each IGAsorp component: gravimetric force (F_G) and buoyant force (F_B). F_G is directed downwards, while F_B is an upward force exerted on an object which is equivalent to the volume of fluid displaced. According to Archimedes' principle, buoyancy can be determined using the following equation:

$$\begin{aligned} F_b &= Buoyancy = gV_i\rho_g(T, RH\ \%) \\ &= g\frac{m_i}{\rho_i}\rho_g(T,\ \%\ RH). \end{aligned} \tag{8}$$

Equation (8) indicates that the buoyancy (F_b) is a function of the temperature and the concentration of the vapor displaced, which is directly related to % RH. The density of the surrounding gas, ρ_g, is estimated using a mole fraction average of water and nitrogen, as shown in Eq. (9), where P_T is the

TABLE II. Standard IGAsorp microbalance components included in the buoyancy correction.

Symbol	Component	Material	Weight (g)	Density (g/cm^3)	Temperature (K)
s	Sample	Variable	m_s	ρ_s	Sample Temp
a	Vapor	H_2O or organics	m_a	ρ_a	Sample Temp
i_1	Sample container	316 SS or Pyrex	m_1	ρ_1	Sample Temp
i_2	Lower sample hook	Tungsten	0.0057	19.04	Sample Temp
i_3	Sample chain	22 Ct. gold	0.0930	11.10	T Profile i
i_4	Sample side balance hook	Tungsten	0.0059	19.04	Balance Temp
j_1	Counterweight (CW)	316 SS	0.3808	7.89	CW Temp
j_2	Lower CW hook	Tungsten	0.0057	19.04	CW Temp
j_3	CW chain	22 Ct. gold	0.0650	11.10	T Profile j
j_4	CW side balance hook	Tungsten	0.0058	19.04	Balance Temp

total pressure and P_{H_2O} and P_{N_2} are the partial pressures of water and nitrogen, respectively:

$$\rho_g = \rho_{H_2O}\, x_{H_2O} + \rho_{N_2} x_{N_2} = \rho_{H_2O}\frac{P_{H_2O}}{P_T} + \rho_{N_2}\frac{P_{N_2}}{P_T}. \tag{9}$$

The partial pressures of water and nitrogen are determined by the relative humidity and temperature conditions, as shown in Eq. (10):

$$\%\,RH = \frac{P_{H_2O}}{P^0(T)} \times 100\%, \tag{10}$$

where $P^0(T)$ is the saturated pressure of water at a specific temperature and is estimated with REFPROP v.9.1[122] using the formulation by Wagner and Pruß.[137] Equations (8) and (9) are applied on the balance components listed in Table II. The temperatures of each component are also included in Table II, and the temperatures for the sample and counterweight chains are described as "T Profile i" and "T Profile j", respectively. Due to the length of the gold chain and its position between different temperature regulated regions in the IGAsorp, the chains are best expressed as having a temperature gradient like those that were described earlier for the IGA balance in Sec. II.

The mass balance for the IGAsorp components is shown in Eq. (11) (where the gravity terms have been canceled out):

$$\begin{aligned} m_{IGAsorp} = {} & \sum_{i=1} m_i + m_s + m_a \sum_{i=1} \frac{m_i}{\rho_i}\rho_g(T_i, RH\%) \\ & - \frac{m_s}{\rho_s}\rho_g(T_s, RH\%) - \frac{m_a}{\rho_a}\rho_g(T_a, RH\%) \\ & - \left(\sum_{j=1} m_j - \sum_{i=j} \frac{m_j}{\rho_j}\rho_g(T_j, RH\%)\right) \\ & - C_f(T_s, RH\%). \end{aligned} \tag{11}$$

Equation (11) includes the sample side components (m_i), the sample (m_s), and the absorbed water (m_a), as shown by the first three terms. The buoyancy effect for these components is subtracted in the next three terms. The contributions by the gravimetric forces on the counterweight side j are subtracted, and the buoyancy contributions of side j are added. Finally, a correction factor term is included to account for the instrument error, and the overall equation results in the mass reported by the IGAsorp ($m_{IGAsorp}$). Since we assume that the volume is additive (as mentioned in Sec. II), Eq. (11) incorporates volume expansion in the third and fifth terms on the right hand side of the equation. The correction factor, C_f, is determined for each temperature and relative humidity point by recording the balance results without a sample. Once C_f is determined, one can solve for m_a from Eq. (11).

Water and temperature can have a large effect on the physical properties of ILs such as viscosity,[138,139] electrochemical properties, and their solvation effects.[140] The sorption and desorption of water in 1-butyl-3-methylimidazolium acetate [bmim][OAc] at 298.85, 300.15, and 315.15 K from 0% to 25% RH has been recently measured by our group. The results for mole fraction of water absorbed as a function of water partial pressure are shown in Fig. 6(a). Our studies clearly show that the sorption of water in [bmim][OAc] is reversible, with no hysteresis, as the sorption and desorption points agree within 0.2%. The results additionally demonstrate the precise and reproducible measurement ability of the IGAsorp instrument. Similar trends are observed when the data are plotted as x_w versus % RH, as shown in Fig. 6(b), indicating that the sorption of water in [bmim][OAc] is solely dependent on the ratio of the water vapor pressure to the saturated water vapor pressure. The uncertainty in solubility measurements was < 0.06 mol.%. The IGAsorp error for the 0–25% RH range is ±1% RH, which is equivalent to ± 82 Pa water partial pressure at 315.15 K.

Other groups have also studied the sorption of water in ILs using the IGAsorp. Dahi *et al.* compared the effects of different cations and anions on water vapor sorption over a wide range of water activity.[141] They also used the IGAsorp with organic solutes to investigate the separation capabilities of supported ionic liquid membranes for water and other organic vapors including cyclohexane and ethanol.[142]

In summary, water is ubiquitous and its impact on materials is yet to be fully understood. Gravimetric vapor sorption

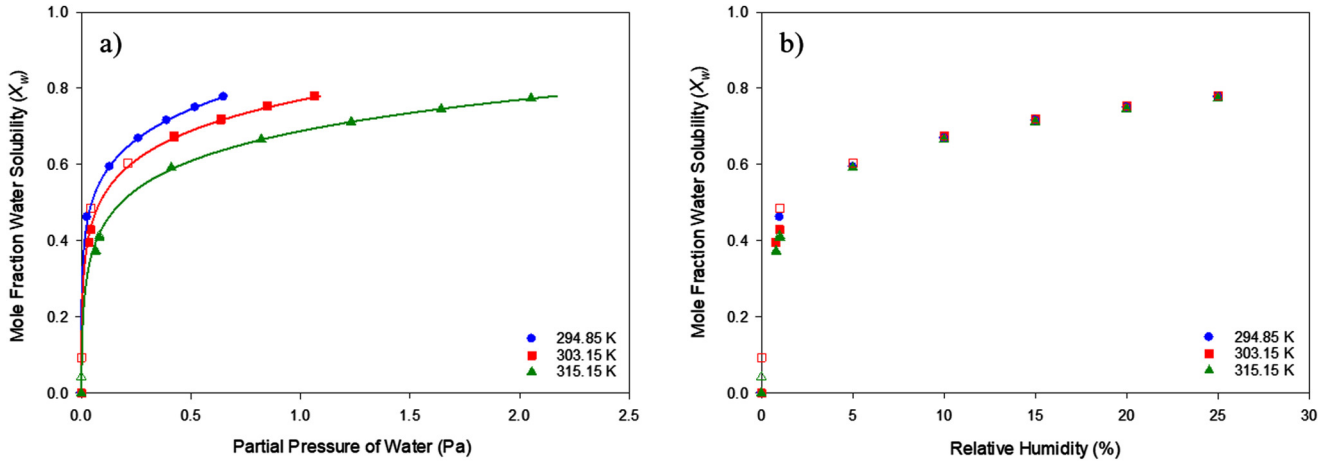

FIG. 6. (a) Water absorption (filled markers) and desorption (empty markers) in [bmim][OAc] as a function of the partial pressure of water from 294.85 to 315.15 K. Empirical curves shown to guide the eye. (b) Isotherms for 294.85–315.15 K of water absorption (filled markers) and desorption (empty markers) in [bmim][OAc] as a function of relative humidity.

analysis is a highly accurate experimental method for assessing the interaction between water and materials.

IV. XEMIS GRAVIMETRIC MICROBALANCE

The XEMIS microbalance is a new design by Hiden which incorporates a magnetically coupled balance allowing higher operating pressures (up to 20 MPa) and the ability to test corrosive gases. The name XEMIS comes from The Greek goddess Themis who holds the scale of justice and whose name means "divine law." The unique symmetric design reduces buoyancy effects and improves measurement accuracy without compromising resolution or stability.

The first studies published using an XEMIS microbalance were by Adeniran and Mokaya in 2015, who investigated CO_2 and H_2 adsorption in carbon nanotubes.[63,70] The XEMIS balance measurements at 77 and 298 K were found to be in good agreement with those obtained using an IGA microbalance at pressures up to 2 MPa.[63,70] The XEMIS has also been used for studying CO_2, H_2, and CH_4 gas storage in a variety of materials ranging from hydrothermally carbonized biomass (hydrochar) to highly porous MOFs.[143–145] The XEMIS has also been used to study gas adsorption in a variety of polymeric membranes for separation applications.[146–152]

The XEMIS can operate over a broad temperature range (77–773 K) and the balance can hold a maximum sample weight of 5 g. The maximum sorption capacity is 200 mg with a weighing resolution of 0.2 μg. The XEMIS, similar to the IGA, can be operated in both "static" and "dynamic" modes. The static mode uses a pair of admit and exhaust valves to regulate pressure, similar to the IGA. The XEMIS can also be set up to handle mixed gas streams. In dynamic mode, a set of mass flow controllers regulate the pressure with automatic switching between inlets to adjust the composition of the mixture. In this mode of operation, the XEMIS can be connected to an on-line mass spectrometer to analyze the gas expelled from the system through the dynamic sampling port (DSP). The DSP comes with a pressure reduction option which reduces pressure to 1 atm (0.1 MPa) when the XEMIS is operating at high pressures. The balance can also be set up for vapor measurements (water or organic solvents) similar to the IGA.

The XEMIS system consists of a balance cabinet, control system, vacuum pump, heating and cooling units, and computer. The cabinet houses the magnetic suspension balance and is held at a temperature of 313.15 K to maintain the balance stability. The cabinet is mounted to the floor on a frame which is designed to minimize vibration. Beneath the balance cabinet are two equal size stainless-steel vessels which contain the sample cup (right side) and counterweight (left side). Gantries inside the vessels support the temperature sensors and protect the hangdown wires. The internal volume of each vessel and the overall volume of the system are approximately 88 and 450 cm^3, respectively. The small internal volume of the XEMIS balance reduces the amount of gas required for each experiment. The control system consists of a temperature control unit, computer interface, valve drivers, and gas handling system. A flow control system can also be added for dynamic mode operations. The control system provides the interface to Hiden's HIsorp software which allows users to easily setup an individual isotherm or sequential experiments including pre- and post-treatments (heat, vacuum, etc.). The interface has real-time processor functions, high resolution graphics with user specific display options, and simple task symbols for easy operation. The HIsorp software also provides warning messages to minimize errors during setup. Experimental data can also be analyzed using the HIsorp software even when the experiment is in progress.

The vacuum system consists of an oil-free backing pump and a turbopump. For normal operations, the backing pump reduces the system pressure to about 10^{-2} MPa and the turbomolecular pump can reduce the pressure down to 10^{-10} MPa. The XEMIS can be set up with a standard furnace (up to 773 K), cryofurnace (down to 77 K), and water bath (278 to 358 K) with temperature regulation accuracy from ± 0.05 (water bath) to 0.1–1.0 K (furnaces). The

XEMIS can also be equipped with multiple sensors for accurately measuring pressure over both low (up to 2 MPa) and high (up to 20 MPa) ranges with an accuracy of 0.04% of transducer range. The upper pressure limit can be specified by the user and if the condition is exceeded, the experiment will stop. In addition, the XEMIS microbalance contains both low and high pressure relief valves as an additional safety precaution.

A schematic of the XEMIS is shown in Fig. 7 with a description of the components which are used in the force balance equation (see Sec. II) provided in Table III. Stainless-steel and nichrome hangdown wires connect the sample and counter weight to the balance. Similar to the IGA, the XEMIS has various size Pyrex containers for liquid samples and stainless-steel micromesh cone containers for solid samples. The microbalance beam is magnetically levitated and is controlled by the exodrive and exosensor mechanisms which are placed outside the pressure chamber, allowing corrosive gases to be tested.

The same methods for correcting buoyancy and volume expansion described in Sec. II are used for the static mode operation of the XEMIS. To minimize the impact of drag forces (F_d) when operating in dynamic mode, Eq. (12) can be included in the buoyancy calculation:

$$F_d = \pm \left(\frac{1}{2} C_d v^2 A \rho_g\right), \tag{12}$$

where C_d is the drag coefficient, v is the gas velocity, A is the effective cross-sectional area for the object in the gas flow, and ρ_g is the gas density.

The solubility of CO_2 in the IUPAC reference ionic liquid [hmim][Tf_2N] was measured using the XEMIS microbalance at 293.15 K over a pressure range from 0 to 5 MPa. The experimental results were in excellent agreement (< 0.5 mol.%) with volumetric measurements by Kumelan *et al.*[120] as shown in Fig. 8.

Time dependent absorption data can also be simultaneously collected in addition to equilibrium solubility for the XEMIS, IGA, and IGAsorp microbalances at each temperature and pressure point. The processes of gas absorbing in a liquid may be highly complex because of possible evolution of heat of mixing, the subsequent liquid convection due to the local temperature difference, as well as the free convection due to the density difference, and the possible change in thermophysical properties of the liquid.[153] However, the effect of such complex phenomena can be minimized with a well-designed experimental setup. Here, we make the following assumptions for the absorbed gas:

(1) Gas absorbs through a one-dimensional (vertical) diffusion process, in which there is no convective flow in the liquid.
(2) A thin boundary layer between the gas and liquid phases exists, where the thermodynamic equilibrium is instantly established with the saturation concentration (C_S), and where the concentration is constant at all times at a given temperature and pressure.
(3) Temperature and pressure are kept constant.

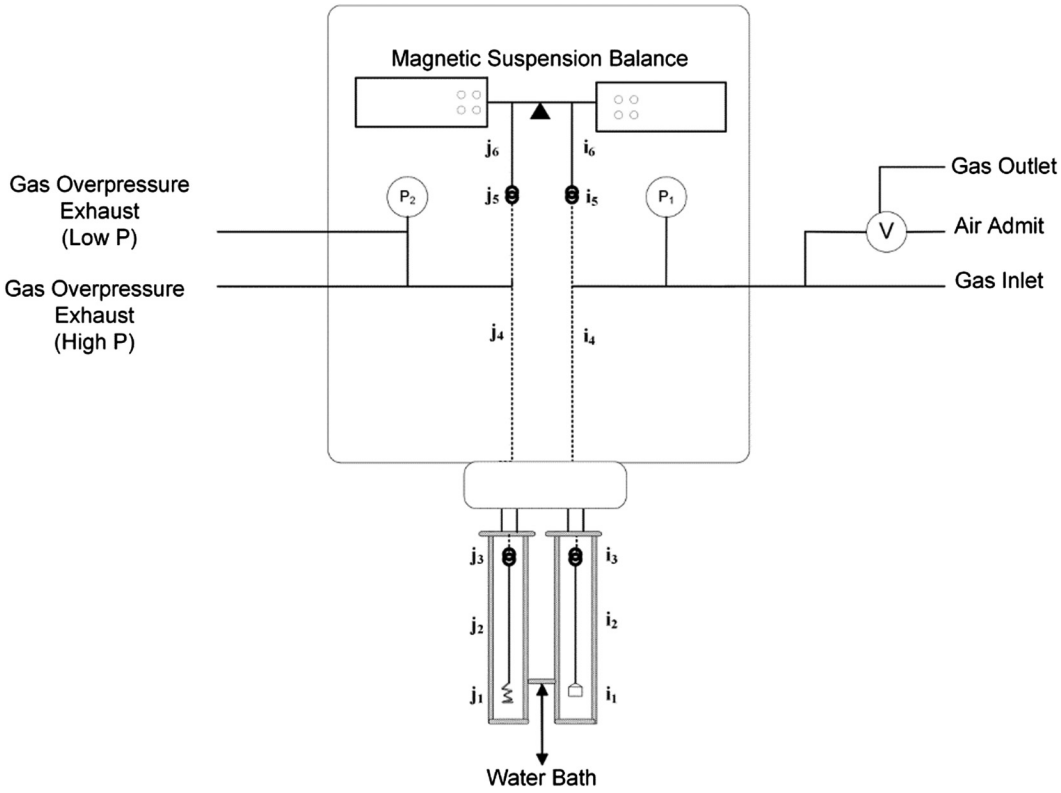

FIG. 7. Hiden XEMIS gravimetric microbalance schematic with component labels. Nomenclature is described in Table III (Ref. 6).

TABLE III. Standard XEMIS microbalance components included in buoyancy correction.

Subscript	Component	Material	Weight (g)	Density (g/cm^3)	Temperature (K)
s	Sample	Variable	m_s	ρ_s	Sample Temp
a	Gas	Variable	m_a	ρ_a	Sample Temp
i_1	Sample container	Pyrex	0.4769	2.23	Sample Temp
i_2	Hangdown	316 SS	0.0214	7.89	Cabinet Temp
i_3	Hook	316 SS	0.0465	7.89	Cabinet Temp
i_4	Hangdown	80% Ni/20% Cr	0.002	8.4	T Profile i
i_5	Hook	316 SS	0.04635	7.89	Cabinet Temp
i_6	Hangdown	316 SS	0.0209	7.89	Cabinet Temp
j_1	Counterweight	316 SS	0.5956	7.89	CW Temp
j_2	Hangdown	316 SS	0.0214	7.89	Cabinet Temp
j_3	Hook	316 SS	0.0462	7.89	Cabinet Temp
j_4	Hangdown	80% Ni/20% Cr	0.002	8.4	T Profile j
j_5	Hook	316 SS	0.04635	7.89	Cabinet Temp
j_6	Hangdown	316 SS	0.021	7.89	Cabinet Temp

(4) The gas-dissolved liquid is a highly dilute solution, and so the relevant thermophysical properties of the solution do not change.

Under these criteria, the process may be described by one-dimensional mass diffusion due to the local concentration difference. The governing differential equation (Fick's second law) is

$$\frac{\partial C}{\partial t} = D\frac{\partial^2 C}{\partial z^2}, \tag{13}$$

with

$$\text{Initial condition: } C = C_0 \text{ when } t = 0 \text{ and } 0 < z < L, \tag{14}$$

$$\text{Boundary conditions: } C = C_S \text{ when } t > 0 \text{ and } z = 0, \tag{15}$$

$$\frac{\partial C}{\partial z} = 0 \text{ at } z = L, \tag{16}$$

where C is the concentration of a dissolving substance in an ionic liquid as a function of time, t, and vertical location, z, where L is the depth of the IL in the container, and $(z = 0)$ corresponds to the vapor–liquid boundary. C_0 is an initial homogenous concentration of the dissolving gas and is zero (initially) or a small finite amount at $t > 0$. D is the diffusion coefficient that is assumed to be constant.

Equation (13) can be solved analytically for the initial and boundary conditions [Eqs. (14)–(16)] using a standard method such as separation of variables or a Laplace transform which yields

$$C = C_S[1 - 2(1 - \frac{C_0}{C_S})\sum_{n=0}^{\infty}\frac{\exp(-\lambda_n^2 D t)\sin\lambda_n z}{L\lambda_n}], \tag{17}$$

where $\lambda_n = (n + 1/2)\pi/L$.

The total concentration (or mass) of dissolved gas in an ionic liquid is an experimentally observed quantity at a specified time and is different from the concentration profile in z. This space-averaged concentration at a given time, $\langle C\rangle$, can be calculated using Eq. (18):

$$\langle C\rangle = \int_0^L C dz/L, \tag{18}$$

$$\langle C\rangle = C_S[1 - 2(1 - \frac{C_0}{C_S})\sum_{n=0}^{\infty}\frac{\exp(-\lambda_n^2 D t)}{L^2\lambda_n^2}]. \tag{19}$$

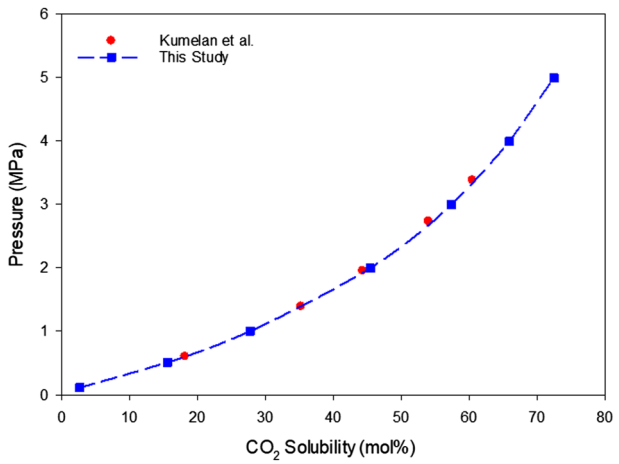

FIG. 8. P–x diagram of the system CO_2 and [hmim][Tf_2N] with isothermal data at 293.15 K. Blue squares represent this study; red circles represent data by Kumełan *et al.* (Ref. 120). The dashed line is provided as a guide for the reader.

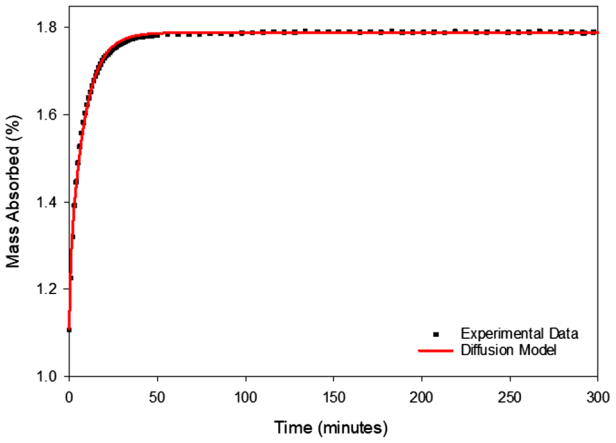

FIG. 9. Comparison of percent mass absorbed with diffusion model for CO_2 and [hmim][Tf_2N] isotherm measured at 293.15 K and 0.5 MPa: symbols present observed data and line calculated with the present diffusion model parameters (Co = 1.11 mass%, D = $1.47 \pm 0.1 \times 10^{-10}$ m^2/s; $C_S = 1.79 \pm 0.01$ mass%).

Although Eq. (19) contains an infinite summation, only the first few terms (i.e., $n = 10$–20) are needed for most applications, except for initial small time periods. For most cases, the summation is terminated after ten terms when the numerical contribution to the summation in $\langle C \rangle$ becomes less than 10^{-12}. Analyzing experimental data with this equation, can obtain the saturation concentration (C_s) and diffusion constant (D) at given T and P, when C_0 is known. However, the analysis requires nonlinear regression, and the best fit is obtained by choosing the proper value for C_0.

The above model was applied to CO_2 absorbing into [hmim][Tf_2N] at 293.15 K and 0.5 MPa as shown in Fig. 9, where the calculated diffusivity $D = 1.47 \pm 0.1 \times 10^{-10}$ m^2 s^{-1} and the calculated saturation concentration $C_S = 1.79 \pm 0.01$ mass percent (or 15.6 ± 0.1 mol.%). The calculated height was $L = 0.434$ mm. The 0.5 MPa set-point is the second pressure set-point to be measured at 293.15 K; therefore, the percent mass absorbed (C_0) begins at 1.11 mass percent (not zero as shown in Fig. 9) due to prior absorption at earlier set-point. In the case given where the sample has been thoroughly evacuated and is ramping to the initial pressure set-point, the initial concentration is $C_0 = 0$. For all other cases, some amount of time is required to ramp in pressure to the next set-point. During the ramp time, the balance weight decreases due to the buoyancy effect which increases with pressure while simultaneous absorption is occurring. The model can only be properly applied once the pressure set-point is reached, at which point (C_0) is not precisely known, in this case the previous value result for (C_S) provides a starting value.

V. SUMMARY

Simple balances have been used for thousands of years. Today, high-precision electronic microbalances can measure extremely small mass changes as a function of temperature, pressure, and gas composition. Hiden Isochema manufactures three automated gravimetric microbalances (IGA, IGAsorp, and XEMIS) for measuring gas and vapor sorption over a wide range in temperature and pressure conditions. This review provides a detailed description of these three instruments and some recent results measuring CO_2 and H_2O sorption in ILs.

ACKNOWLEDGMENTS

The authors would like to thank Mark Roper, Darren Broom, and Michael Benham at Hiden Isochema (Warrington, U.K.) for their support in establishing a state-of-the-art gravimetric microbalance laboratory at The University of Kansas and assistance with references for this paper. The authors would also like to thank Luke Wilkinson and Dave Goodier for assistance with setting up the IGA and XEMIS microbalances, Mohammed (Mo) Akhtar for assistance with setting up the IGAsorp microbalance, and Katherine McKie, Matt Gee, and Mathew Powner for customer assistance.

[1]E. Robens, S. A. A. Jayaweera, and S. Kiefer, *Balances Instruments, Manufacturers, History* (Springer-Verlag GmbH, Heidelberg Germany, 2014).
[2]W. C. Pierce, E. L. Haenisch, and D. T. Sawyer, *Quantitative Analysis*, edited by W. C. Pierce, E. L. Haenisch, and D. T. Sawyer, 4th ed. (Wiley, New York, 1958), Vol. 497, p. Xiii.
[3]F. Willis, ACS Today's Chem. Work **45,** 45 (2004).
[4]M. J. Benham and D. K. Ross, Zeitschrift Fur Phys. Chemie Neue Folge **163**, 25 (1989).
[5]M. B. Shiflett and A. Yokozeki, Ind. Eng. Chem. Res. **44**, 4453 (2005).
[6]M. B. Shiflett and E. J. Maginn, Aiche J. **63**, 4722 (2017).
[7]A. J. Fletcher and K. M. Thomas, Langmuir **16**, 6253 (2000).
[8]R. Van der Vaart, C. Huiskes, H. Bosch, and T. Reith, Adsorpt. Int. Adsorpt. Soc. **6**, 311 (2000).
[9]X. B. Zhao, B. Xiao, A. J. Fletcher, and K. M. Thomas, J. Phys. Chem. B **109**, 8880 (2005).
[10]Z. X. Yang, Y. D. Xia, X. Z. Sun, and R. Mokaya, J. Phys. Chem. B **110**, 18424 (2006).
[11]X. B. Zhao, S. Villar-Rodil, A. J. Fletcher, and K. M. Thomas, J. Phys. Chem. B **110**, 9947 (2006).
[12]X. H. Shao, W. C. Wang, and X. J. Zhang, Carbon N.Y. **45**, 188 (2007).
[13]Z. X. Yang, Y. D. Xia, and R. Mokaya, J. Am. Chem. Soc. **129**, 1673 (2007).
[14]O. Czakkel, G. Onyestyak, G. Pilatos, V. Kouvelos, N. Kanellopoulos, and K. Laszlo, Microporous Mesoporous Mater. **120**, 76 (2009).
[15]G. Srinivas, Y. W. Zhu, R. Piner, N. Skipper, M. Ellerby, and R. Ruoff, Carbon N.Y. **48**, 630 (2010).
[16]N. Alam and R. Mokaya, Microporous Mesoporous Mater. **142**, 716 (2011).
[17]N. Alam and R. Mokaya, Microporous Mesoporous Mater. **144**, 140 (2011).
[18]M. Sevilla, A. B. Fuertes, and R. Mokaya, Int. J. Hydrogen Energy **36**, 15658 (2011).
[19]X. H. Shao, Z. H. Feng, R. S. Xue, C. C. Ma, W. C. Wang, X. Peng, and D. P. Cao, AIChE J. **57**, 3042 (2011).
[20]Y. D. Xia, R. Mokaya, D. M. Grant, and G. S. Walker, Carbon N.Y. **49**, 844 (2011).
[21]H. W. Yang, Y. Z. Yuan, and S. C. E. Tsang, Chem. Eng. J. **185**, 374 (2012).
[22]A. J. Fletcher, E. J. Cussen, T. J. Prior, M. J. Rosseinsky, C. J. Kepert, and K. M. Thomas, J. Am. Chem. Soc. **123**, 10001 (2001).
[23]J. Mugge, H. Bosch, and T. Reith, Chem. Eng. Sci. **56**, 5351 (2001).
[24]A. J. Fletcher, E. J. Cussen, D. Bradshaw, M. J. Rosseinsky, and K. M. Thomas, J. Am. Chem. Soc. **126**, 9750 (2004).
[25]X. B. Zhao, B. Xiao, A. J. Fletcher, K. M. Thomas, D. Bradshaw, and M. J. Rosseinsky, Science. **306**, 1012 (2004).
[26]S. M. Hawxwell, G. M. Espallargas, D. Bradshaw, M. J. Rosseinsky, T. J. Prior, A. J. Florence, J. van de Streek, and L. Brammer, Chem. Commun. **15**, 1532 (2007).

[27]J. H. Jia, X. Lin, C. Wilson, A. J. Blake, N. R. Champness, P. Hubberstey, G. Walker, E. J. Cussen, and M. Schroder, Chem. Commun. 840 (2007).
[28]B. Xiao *et al.*, J. Am. Chem. Soc. **129**, 1203 (2007).
[29]B. L. Chen, X. Zhao, A. Putkham, K. Hong, E. B. Lobkovsky, E. J. Hurtado, A. J. Fletcher, and K. M. Thomas, J. Am. Chem. Soc. **130**, 6411 (2008).
[30]S. Yang, X. Lin, A. J. Blake, K. M. Thomas, P. Hubberstey, N. R. Champness, and M. Schroder, Chem. Commun. **46**, 6108 (2008).
[31]X. Lin *et al.*, J. Am. Chem. Soc. **131**, 2159 (2009).
[32]K. J. Msayib *et al.*, Angew. Chem. Int. Ed. **48**, 3273 (2009).
[33]Z. H. Xiang, J. H. Lan, D. P. Cao, X. H. Shao, W. C. Wang, and D. P. Broom, J. Phys. Chem. C **113**, 15106 (2009).
[34]B. Xiao *et al.*, Nat. Chem. **1**, 289 (2009).
[35]Y. Yan, X. Lin, S. H. Yang, A. J. Blake, A. Dailly, N. R. Champness, P. Hubberstey, and M. Schroder, Chem. Commun. **9**, 1025 (2009).
[36]I. A. Ibarra *et al.*, Chem. Eur. J. **16**, 13671 (2010).
[37]Z. J. Liang, M. Marshall, and A. L. Chaffee, Microporous Mesoporous Mater. **132**, 305 (2010).
[38]H. Wu *et al.*, Chem. Eur. J. **16**, 5205 (2010).
[39]Z. H. Xiang, D. P. Cao, X. H. Shao, W. C. Wang, J. W. Zhang, and W. Z. Wu, Chem. Eng. Sci. **65**, 3140 (2010).
[40]S. Sircar, H. H. Wu, J. Li, and A. D. Lueking, Langmuir **27**, 14169 (2011).
[41]P. D. Southon, D. J. Price, P. K. Nielsen, C. J. McKenzie, and C. J. Kepert, J. Am. Chem. Soc. **133**, 10885 (2011).
[42]K. C. Stylianou, J. E. Warren, S. Y. Chong, J. Rabone, J. Bacsa, D. Bradshaw, and M. J. Rosseinsky, Chem. Commun. **47**, 3389 (2011).
[43]Z. H. Xiang, Z. Hu, D. P. Cao, W. T. Yang, J. M. Lu, B. Y. Han, and W. C. Wang, Angew. Chem. Int. Ed. **50**, 491 (2011).
[44]Z. X. Zhao, X. M. Li, and Z. Li, Chem. Eng. J. **173**, 150 (2011).
[45]J. Liu, J. Tian, P. K. Thallapally, and B. P. McGrail, J. Phys. Chem. C **116**, 9575 (2012).
[46]M. T. Wharmby *et al.*, Microporous Mesoporous Mater. **157**, 3 (2012).
[47]Z. H. Xiang, Z. Hu, W. T. Yang, and D. P. Cao, Int. J. Hydrogen Energy **37**, 946 (2012).
[48]S. H. Yang *et al.*, Nat. Mater. **11**, 710 (2012).
[49]I. P. OKoye, M. Benham, and K. M. Thomas, Langmuir **13**, 4054 (1997).
[50]C. R. Reid, I. P. O'koye, and K. M. Thomas, Langmuir **14**, 2415 (1998).
[51]C. R. Reid and K. M. Thomas, Langmuir **15**, 3206 (1999).
[52]J. Peng, H. Y. Ban, X. T. Zhang, L. J. Song, and Z. L. Sun, Chem. Phys. Lett. **401**, 94 (2005).
[53]M. Palomino, A. Cantin, A. Corma, S. Leiva, F. Rey, and S. Valencia, Chem. Commun. **12**, 1233 (2007).
[54]B. J. Dou, Q. Hu, J. J. Li, S. Z. Qiao, and Z. P. Hao, J. Hazard. Mater. **186**, 1615 (2011).
[55]H. W. Yang, A. M. Khan, Y. Z. Yuan, and S. C. Tsang, Chem. Asian J. **7**, 498 (2012).
[56]M. D. Macedonia, D. D. Moore, E. J. Maginn, and M. M. Olken, Langmuir **16**, 3823 (2000).
[57]A. Berenguer-Murcia, A. J. Fletcher, J. Garcia-Martinez, D. Cazorla-Amoros, A. Linares-Solano, and K. M. Thomas, J. Phys. Chem. B **107**, 1012 (2003).
[58]H. W. Langmi, D. Book, A. Walton, S. R. Johnson, M. M. Al-Mamouri, J. D. Speight, P. P. Edwards, I. R. Harris, and P. A. Anderson, J. Alloys Compd. **404**, 637 (2005).
[59]H. W. Langmi *et al.*, J. Alloys Compd. **356**, 710 (2003).
[60]T. A. Steriotis, K. L. Stefanopoulos, F. K. Katsaros, R. Glaser, A. C. Hannon, and J. D. F. Ramsay, Phys. Rev. B **78**, 115424 (2008).
[61]J. J. Gutierrez-Sevillano, D. Dubbeldam, F. Rey, S. Valencia, M. Palomino, A. Martin-Calvo, and S. Calero, J. Phys. Chem. C **114**, 14907 (2010).
[62]S. Tedds, A. Walton, D. P. Broom, and D. Book, Faraday Discuss. **151**, 75 (2011).
[63]B. Adeniran and R. Mokaya, J. Mater. Chem. A **3**, 5148 (2015).
[64]A. Hanif, S. Dasgupta, and A. Nanoti, Ind. Eng. Chem. Res. **55**, 8070 (2016).
[65]A. Hanif, S. Dasgupta, S. Divekar, A. Arya, M. O. Garg, and A. Nanoti, Chem. Eng. J. **236**, 91 (2014).
[66]C. P. Krap *et al.*, Inorg. Chem. **55**, 1076 (2016).
[67]W. Wong-Ng, J. T. Culp, Y. S. Chen, J. R. Deschamps, and A. Marti, Solid State Sci. **52**, 1 (2016).
[68]S. A. Li, Y. X. Shi, H. Y. Zeng, and N. S. Cai, Adsorpt. Int. Adsorpt. Soc. **23**, 239 (2017).
[69]C. M. Moran, R. M. Marti, S. E. Hayes, and K. S. Walton, Carbon N.Y. **114**, 482 (2017).
[70]B. Adeniran and R. Mokaya, Nano Energy **16**, 173 (2015).
[71]R. Swaidan, B. Ghanem, M. Al-Saeedi, E. Litwiller, and I. Pinnau, Macromolecules **47**, 7453 (2014).
[72]O. Salinas, X. H. Ma, E. Litwiller, and I. Pinnau, J. Memb. Sci. **504**, 133 (2016).
[73]O. Salinas, X. H. Ma, Y. G. Wang, Y. Han, and I. Pinnau, RSC Adv. **7**, 3265 (2017).
[74]J. Q. Liu *et al.*, Carbon N.Y. **123**, 273 (2017).
[75]K. J. Kim, P. Lu, J. T. Culp, and P. R. Ohodnicki, ACS Sensors **3**, 386 (2018).
[76]X. X. Wu, Z. W. Tian, L. Q. Hu, S. Huang, and J. J. Cai, RSC Adv. **7**, 32795 (2017).
[77]R. Vakili, S. J. Xu, N. Al-Janabi, P. Gorgojo, S. M. Holmes, and X. L. Fan, Microporous Mesoporous Mater. **260**, 45 (2018).
[78]N. J. Foley, K. M. Thomas, P. L. Forshaw, D. Stanton, and P. R. Norman, Langmuir **13**, 2083 (1997).
[79]L. Cossarutto, T. Zimny, J. Kaczmarczyk, T. Siemieniewska, J. Bimer, and J. V. Weber, Carbon N.Y. **39**, 2339 (2001).
[80]V. Detallante, D. Langevin, C. Chappey, M. Metayer, R. Mercier, and M. Pineri, Desalination **148**, 333 (2002).
[81]V. Detallante, D. Langevin, C. Chappey, M. Metayer, R. Mercier, and M. Pineri, J. Memb. Sci. **190**, 227 (2001).
[82]D. J. Allardice, L. M. Clemow, G. Favas, W. R. Jackson, M. Marshall, and R. Sakurovs, Fuel **82**, 661 (2003).
[83]V. Dubey, S. Kuthe, C. Saxena, and D. K. Jaiswal, J. Appl. Polym. Sci. **88**, 1760 (2003).
[84]V. Dubey, L. K. Pandey, and C. Saxena, J. Memb. Sci. **251**, 131 (2005).
[85]M. Ghodhbene, F. Bougie, P. Fongarland, and M. C. Iliuta, Can. J. Chem. Eng. **95**, 1842 (2017).
[86]E. C. Vermisoglou, V. Georgakilas, E. Kouvelos, G. Pilatos, K. Viras, G. Romanos, and N. K. Kanellopoulos, Microporous Mesoporous Mater. **99**, 98 (2007).
[87]Z. S. Seddegi, U. Budrthumal, A. A. Al-Arfaj, A. M. Al-Amer, and S. A. I. Barri, Appl. Catal. A-General **225**, 167 (2002).
[88]J. Nastaj and T. Aleksandrzak, J. Chem. Eng. Data **58**, 2629 (2013).
[89]S. K. Xian, Y. Yu, J. Xiao, Z. J. Zhang, Q. B. Xia, H. H. Wang, and Z. Li, RSC Adv. **5**, 1827 (2015).
[90]X. L. Tan, L. Vagi, Q. Liu, P. Choi, and M. R. Gray, Can. J. Chem. Eng. **94**, 220 (2016).
[91]G. Gatti, D. F. O. Olivera, V. Sacchetto, M. Cossi, I. Braschi, L. Marchese, and C. Bisio, Chemphyschem **18**, 2374 (2017).
[92]K. A. Lukaszuk *et al.*, Catal. Sci. Technol. **7**, 5435 (2017).
[93]X. F. Qian, M. Ren, D. T. Yue, Y. Zhu, Y. Han, Z. F. Bian, and Y. X. Zhao, Appl. Catal. B –Environ. **212**, 1 (2017).
[94]A. J. Fletcher, M. J. Benham, and K. M. Thomas, J. Phys. Chem. B **106**, 7474 (2002).
[95]J. U. Keller, and R. Staudt, *Gas Adsorption Equilibria: Experimental Methods and Adsorptive Isotherms* (Springer, New York, 2005).
[96]P. A. Chater, P. A. Anderson, J. W. Prendergast, A. Walton, V. S. J. Mann, D. Book, W. I. F. David, S. R. Johnson, and P. P. Edwards, J. Alloys Compd. **446**, 350 (2007).
[97]J. A. Turner and K. M. Thomas, Langmuir **15**, 6416 (1999).
[98]M. W. Ma, L. Wang, Y. Wang, W. Xiang, P. Lyu, B. H. Tang, and X. H. Tan, J. Alloys Compd. **709**, 445 (2017).
[99]M. W. Ma, W. Xiang, B. H. Tang, L. Liang, L. Wang, and X. H. Tan, J. Nucl. Mater. **467**, 349 (2015).
[100]J. L. Anthony, E. J. Maginn, and J. F. Brennecke, J. Phys. Chem. B **106**, 7315 (2002).
[101]J. L. Anthony, E. J. Maginn, and J. F. Brennecke, J. Phys. Chem. B **105**, 10942 (2001).
[102]C. Cadena, J. L. Anthony, J. K. Shah, T. I. Morrow, J. F. Brennecke, and E. J. Maginn, J. Am. Chem. Soc. **126**, 5300 (2004).
[103]L. F. Lepre, L. Pison, L. J. A. Siqueira, R. A. Ando, and M. F. C. Gomes, Sep. Purif. Technol. **196**, 10 (2018).
[104]L. F. Lepre, J. Szala-Bilnik, L. Pison, M. Traikia, A. A. H. Padua, R. A. Ando, and M. F. C. Gomes, Phys. Chem. Chem. Phys. **19**, 12431 (2017).
[105]M. Mohamedali, H. Ibrahim, and A. Henni, Chem. Eng. J. **334**, 817 (2018).
[106]M. Zoubeik, M. Mohamedali, and A. Henni, Fluid Phase Equilib. **419**, 67 (2016).

[107]Z. G. Lei, C. N. Dai, and B. H. Chen, Chem. Rev. **114**, 1289 (2014).
[108]M. B. Shiflett, M. A. Harmer, C. P. Junk, and A. Yokozeki, J. Chem. Eng. Data **51**, 483 (2006).
[109]M. B. Shiflett, M. A. Harmer, C. R. Junk, and A. Yokozeki, Fluid Phase Equilib. **242**, 220 (2006).
[110]M. B. Shiflett and A. Yokozeki, Aiche J. **52**, 1205 (2006).
[111]M. B. Shiflett and A. Yokozeki, Ind. Eng. Chem. Res. **45**, 6375 (2006).
[112]M. B. Shiflett and A. Yokozeki, J. Chem. Eng. Data **52**, 2007 (2007).
[113]M. B. Shiflett and A. Yokozeki, J. Chem. Eng. Data **53**, 492 (2008).
[114]M. B. Shiflett, A. D. Shiflett, and A. Yokozeki, Sep. Purif. Technol. **79**, 357 (2011).
[115]M. B. Shiflett, D. R. Corbin, B. A. Elliott, and A. Yokozeki, J. Chem. Thermodyn. **64**, 40 (2013).
[116]M. B. Shiflett, D. R. Corbin, and A. Yokozeki, Adsorpt. Sci. Technol. **31**, 59 (2013).
[117]See: https://www.Iupac.Org/Publications/Ci/2005/2705/Pp4_2002-005-1-100.html (2002).
[118]M. B. Shiflett and A. Yokozeki, J. Phys. Chem. B **111**, 2070 (2007).
[119]M. F. C. Gomes, J. Chem. Eng. Data **52**, 472 (2007).
[120]J. Kumelan, I. P. S. Kamps, D. Tuma, and G. Maurer, J. Chem. Thermodyn. **38**, 1396 (2006).
[121]B. Shirani and M. Eic, Ind. Eng. Chem. Res. **56**, 1008 (2017).
[122]E. W. Lemmon, M. L. Huber, and M. O. Mclinden, NIST Stand. Ref. Database (2013).
[123]W. Ren and A. M. Scurto, Rev. Sci. Instrum. **78**, 125104 (2007).
[124]K. Robertson and D. Bish, J. Geophys. Res. **116**, E07006 (2011).
[125]J. Wang, D. Trinkle, G. Derbin, K. Martin, S. Sharif, P. Timmins, and D. Desai, J. Excipients Food Chem. **5**, 21 (2014).
[126]M. Drobota, L. M. Gradinaru, C. Ciobanu, and D. S. Vasilescu, UPB Sci. Bull. Ser. B Chem. Mater. Sci. **77**, 131 (2015).
[127]C. Tugui, S. Vlad, M. Iacob, C. D. Varganici, L. Pricop, and M. Cazacu, Polym. Chem **7**, 2709 (2016).
[128]M. Cazacu, M. Ignat, C. Racles, M. Cristea, V. Musteata, D. Ovezea, and D. Lipcinski, J. Compos. Mater. **48**, 1533 (2014).
[129]A. Bele, G. Stiubianu, C. D. Varganici, M. Ignat, and M. Cazacu, J. Mater. Sci. **50**, 6822 (2015).
[130]Z. Pásztory, T. Horváth, S. V. Glass, and S. L. Zelinka, For. Prod. J. **65**, 352 (2015).
[131]D. Filip, D. Macocinschi, C. G. Tuchilus, S. Vlad, M. F. Zaltariov, and C. D. Varganici, Polym. Bull. **75**, 701 (2018).
[132]D. Filip, D. Macocinschi, E. Paslaru, C. G. Tuchilus, and S. Vlad, React. Funct. Polym. **102**, 70 (2016).
[133]S. J. Harley, E. A. Glascoe, J. P. Lewicki, and R. S. Maxwell, ChemPhysChem **15**, 1809 (2014).
[134]S. Vlad, L. M. Gradinarli, C. Ciobanu, D. Macocinschi, D. Filip, I. Spiridon, and R. V. Gradinaru, Cellul. Chem. Technol. **49**, 905 (2015).
[135]C. Boardman and S. V. Glass, J. Build. Phys. **38**, 389 (2015).
[136]M. B. Shiflett and A. Yokozeki, *Ion. Liq. Uncoiled* (Wiley, Hoboken, NJ, 2012), pp. 349–386.
[137]W. Wagner and A. Pruß, J. Phys. Chem. Ref. Data **31**, 387 (2002).
[138]K. R. Seddon, A. Stark, and M.-J. Torres, Pure Appl. Chem **72**, 2275 (2000).
[139]M. S. Kelkar and E. J. Maginn, J. Phys. Chem. B **111**, 4867 (2007).
[140]Y. Kohno and H. Ohno, Chem. Commun. Chem. Commun. **48**, 7119 (2012).
[141]A. Dahi, K. Fatyeyeva, C. Chappey, D. Langevin, S. P. Rogalsky, O. P. Tarasyuk, and S. Marais, RSC Adv. **5**, 76927 (2015).
[142]A. Dahi, K. Fatyeyeva, D. Langevin, C. Chappey, S. P. Rogalsky, O. P. Tarasyuk, A. Benamor, and S. Marais, J. Memb. Sci. **458**, 164 (2014).
[143]M. Sevilla, W. Sangchoom, N. Balahmar, A. B. Fuertes and R. Mokaya, ACS Sustain. Chem. Eng. **4**, 4710 (2016).
[144]M. Savage *et al.*, J. Am. Chem. Soc. **138**, 9119 (2016).
[145]M. Savage *et al.*, Adv. Mater. **28**, 8705 (2016).
[146]Y. Xiao, L. Zhang, L. Xu, and T. S. Chung, J. Memb. Sci. **521**, 65 (2017).
[147]J. Liu, Y. Xiao, K. Liao, and T. S. Chung, J. Memb. Sci. **523**, 92 (2017).
[148]W. Yong and T. S. Chung, J. Polym. Sci. Part B Polym. Phys. **55**, 344 (2017).
[149]J. Liu, Y. Xiao, and T. S. Chung, J. Mater. Chem. A **5**, 4583 (2017).
[150]K. Liao, S. Japip, J. Lai, and T. S. Chung, J. Memb. Sci. **534**, 92 (2017).
[151]W. F. Yong, Y. X. Ho, and T. S. Chung, ChemSusChem **10**, 4046 (2017).
[152]A. Naderi, W. Yong, Y. Xiao, T. S. Chung, M. Weber, and C. Maletzko, Polymer (Guildf) **135**, 76 (2018).
[153]M. B. Shiflett and A. Yokozeki, Ind. Eng. Chem. Res. **44**, 4453 (2005).